FULL NUMERICAL QUADRATURE IN GALERKIN BOUNDARY ELEMENT METHODS

Jorge D'Elía, Laura Battaglia, Alberto Cardona and Mario A. Storti

Centro Internacional de Métodos Computacionales en Ingeniería (CIMEC), Instituto de Desarrollo Tecnológico para la Industria Química (INTEC), Universidad Nacional del Litoral - CONICET , Güemes 3450, 3000-Santa Fe, Argentina, e-mail: (jdelia, mstorti)@intec.unl.edu.ar, lbattaglia@santafe-conicet.gov.ar, web page: http://www.cimec.org.ar

Abstract. When a Galerkin discretization of a boundary integral equation with a weakly singular kernel is performed over triangles, a double surface integral must be evaluated for each pair of them. If these pairs are not contiguous or not coincident the kernel is regular and a Gauss–Legendre quadrature can be employed. When the pairs have a common edge or a common vertex, then edge and vertex weak singularities appear. If the pairs have both facets coincident the whole integration domain is weakly singular. D. J. Taylor (IEEE Trans. on Antennas and Propagation, 51(7):1630–1637 (2003)) proposed a systematic evaluation based on a reordering and partitioning of the integration domain, together with a use of the Duffy transformations in order to remove the singularities, in such a way that a Gauss–Legendre quadrature was performed on three coordinates with an analytic integration in the fourth coordinate. Since this scheme is a bit restrictive because it was designed for electromagnetic wave propagation kernels, a full numerical quadrature on the four coordinates is proposed in order to handle kernels with a weak singularity with a general framework. Numerical tests based on modifications of the one proposed by W. Wang and N. Atalla (Comm. in Num. Meth. Eng., 13(11):885–890 (1997)) are included.

1 INTRODUCTION

Integral boundary equations are usually solved with the Boundary Element Method (BEM), e.g. see (París and Cañas, 1997; Hartmann, 1989). Typically, collocation techniques are employed, for instance, for modelling creeping (or Stokes) flows (Power and Wrobel, 1995; Kim and Karrila, 1989) as in (Fachinotti et al., 2007) where fast integration is performed while self–integrals, that contain singular kernels, are analytically computed over linear triangles. Also, closed forms following a side local frame strategy can be employed (Medina and Liggett, 1988; D'Elía et al., 2000a,b), where the surface integral over each panel is replaced by its closed contour integration, and a side local frame is used for each side contribution. Another alternatives are also possible like the so called Galerkin Boundary Element Method (GBEM) or Variational Boundary Element Method (VBEM), e.g. (Paquay, 2002). When this procedure is made with boundary elements (or panels) in the three dimensional Euclidean real space (3D or $\mathbb{R}^3$), it leads to compute double surface integrals, i.e. quadruple integrals, that account for the pairwise interaction among all the panels of the surface mesh, a task that is carried out through a double nested loop $p, q = 1, 2, ..., E$, where E is the number of elements in the boundary mesh.

The generic pair of interacting triangles is the support of the double surface integral, and the integral value gives the interaction coefficient between pairs of triangles, whose multiplicative kernel is obtained as the product of both panel kernels. The interaction coefficient can be either a real or a complex value as well as it can have a scalar or a tensorial character, according to the nature of the Green function. Each panel kernel is related to the Green function of the problem or its derivatives, e.g. as those in creeping flows in Micro-Electro-Mechanical Systems (MEMS) (Wang, 2002; Méndez et al., 2008), acoustics (Schuhmacher, 2000), free surface flows (D'Elía et al., 2000c, 2002a) or seakeeping (D'Elía et al., 2002b), among other computational physics applications. The solutions obtained with VBEM can be also used for testing other numerical formulations like those that solve the Navier–Stokes equations through distributed computing (PETSc-FEM, 2008; Dalcín et al., 2007; Franck et al., 2007) in several contexts, for instance, wave-resistance with absorbing boundary conditions (Storti et al., 1998a, 2008, 1998b), sloshing (Battaglia et al., 2006; Garibaldi et al., 2008), inertial waves (D'Elía et al., 2006) and added mass computations (Storti and D'Elía, 2004).

In the case of kernels with a weak singularity, there are analytical expressions of the double surface integrals in rather restricted cases, for instance, the "potential integrals" (and self–integrals) in computational electromagnetics (Eibert and Hansen, 1995; Sievers et al., 2005), which are designed for flat triangles but restricted to numerator kernels with a constant or linear layer density.

If two interacting triangles are not contiguous or not coincident, then the multiplicative kernel is regular and a Gauss–Legendre quadrature formula can be used. However, when these triangles have a common edge or a common vertex, then there are edge and vertex singularities, respectively. In the case of self–integrals, when both facets are coincident, the whole integration domain is weakly singular. For these reasons, special methods for the numerical integration are proposed in the literature, e.g. the edge singularity case in collocation techniques (Burghignoli et al., 2004).

D. J. Taylor (Taylor, 2003a,b) developed a systematic way for handling double surface integrals with flat triangular elements, based on a convenient reordering of the four iterate integrations that moves the weak singularity to the origin of the four dimensional Euclidean real space (4D or $\mathbb{R}^4$) and, then, uses systematically the Duffy transformation (Duffy, 1982), i.e. regularize the integrand by using polar coordinates. Thus, Taylor chooses a Gauss–Legendre numerical
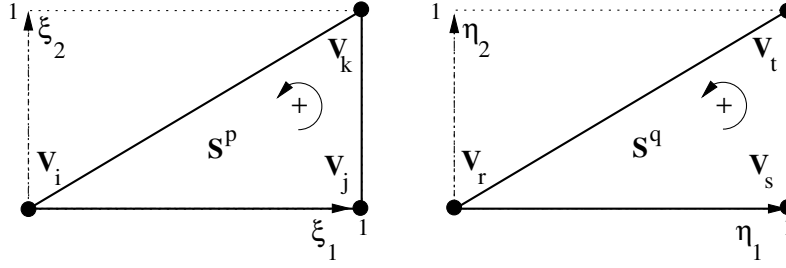
Figure 1: Master triangle for the simplex coordinates.

quadrature on three coordinates and makes an analytic integration in the fourth one.

This Taylor scheme is a bit restrictive since it is specific for wave propagation kernels in computational electromagnetics. A modification is proposed in this work, where a full numerical quadrature on the four coordinates is chosen in order to handle kernels with a weak singulkarity with a general framework. Besides, some technical details missing in the work of Taylor are clarified, as the integration extremes of the iterated integrals after the several coordinates changes introduced to move the singularities to the origin of the integration domain in $\mathbb{R}^4$. For the sake of simplicity only the scalar case is shown although the same procedure can be applied to Green functions of higher tensorial order without any changes. This procedure can be also of interest in VBEM as used, for instance, in fluid-structure-interaction (Paquay, 2002) or acoustics (Schuhmacher, 2000).

2 TRANSFORMATION TO SIMPLEX COORDINATES

The interaction integral Z_{pq} between the p and q panels immersed in $\mathbb{R}^3$ is written as

$$Z^{pq} = \int_{A^p} \mathrm{d}A_{\mathbf{x}}^p \int_{A^q} \mathrm{d}A_{\mathbf{y}}^q \, f(\mathbf{x}, \mathbf{y}) \,, \tag{1}$$

where A^p and A^q are their corresponding surfaces. This is a quadruple integral since it must be evaluated on both panel surfaces, where the integration points $\mathbf{x}$ and $\mathbf{y}$ belong to the p and q panels, respectively. The integrand contains the multiplicative kernel $f = hg$, with $h = h(\mathbf{x}, \mathbf{y})$ being some regular function and $g = g(r)$ is a Green function, where $r = \|\mathbf{x} - \mathbf{y}\|_2$ is the Euclidean distance between the integration points $\mathbf{x}$ and $\mathbf{y}$. It is assumed that the panels p and q are flat triangles and the Green function has only a weak singularity, i.e. $O(1/r)$.

On each panel of the quadruple integral given by Eq. (1), the Cartesian coordinates $\mathbf{x}, \mathbf{y} \in \mathbb{R}^3$ can be transformed into $\mathbb{R}^2$ simplex coordinates. For this aim, two simplex coordinate sets are employed, the (ξ_1, ξ_2) coordinates over the p panel and the (η_1, η_2) ones over the q panel,

$$(\xi_1, \xi_2) : 0 \le \xi_1 \le 1 \; ; \; 0 \le \xi_2 \le \xi_1 \,, \tag{2}$$

$$(\eta_1, \eta_2) : 0 \le \eta_1 \le 1 \; ; \; 0 \le \eta_2 \le \eta_1 \,, \tag{3}$$

see Fig. 1. The generic points on each of these triangles are transformed to the p and q panels using

$$\mathbf{x}(\xi_1, \xi_2) = \mathbf{N}^p(\xi_1, \xi_2)\mathbf{V}^p \,, \tag{4}$$

$$\mathbf{y}(\eta_1, \eta_2) = \mathbf{N}^q(\eta_1, \eta_2)\mathbf{V}^q \,, \tag{5}$$

with the element shape functions

$$\mathbf{N}^p(\xi_1, \xi_2) = \begin{bmatrix} (1 - \xi_1) & (\xi_1 - \xi_2) & \xi_2 \end{bmatrix} \,, \tag{6}$$

$$\mathbf{N}^q(\eta_1, \eta_2) = \begin{bmatrix} (1 - \eta_1) & (\eta_1 - \eta_2) & \eta_2 \end{bmatrix} \,, \tag{7}$$
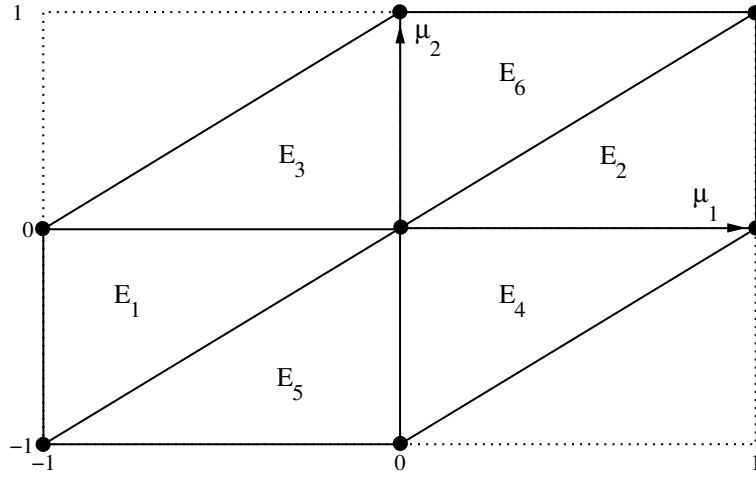
Figure 2: Integration region in the plane of the relative coordinates μ_1, μ_2.

and the element nodal coordinates at the triangle vertices

$$\mathbf{V}^p = \begin{bmatrix} \mathbf{V}_i \\ \mathbf{V}_j \\ \mathbf{V}_k \end{bmatrix} \quad ; \quad \mathbf{V}^q = \begin{bmatrix} \mathbf{V}_r \\ \mathbf{V}_s \\ \mathbf{V}_t \end{bmatrix} . \tag{8}$$

Then, Eq. (1) is written as

$$Z^{pq} = \int_{A^p} \mathrm{d}A^p_{\mathbf{x}} \int_{A^q} \mathrm{d}A^q_{\mathbf{y}} \, f(\mathbf{x}, \mathbf{y}) = J^p J^q \, I \,, \tag{9}$$

where $J^{p,q} = 2A^{p,q}$ are the Jacobians of each panel, and $A^{p,q}$ are their areas, respectively, and the interaction integral I in simplex coordinates is

$$I = \int_0^1 \mathrm{d}\xi_1 \int_0^{\xi_1} \mathrm{d}\xi_2 \int_0^1 \mathrm{d}\eta_1 \int_0^{\eta_1} \mathrm{d}\eta_2 \, f(\boldsymbol{\xi}, \boldsymbol{\eta}) \,. \tag{10}$$

3   DOMAIN DECOMPOSITION FOR CONTIGUOUS OR COINCIDENT FACETS

In the Taylor strategy, when the pair of interacting triangles is contiguous or the triangles are coincident, Eq. (10) is split into six independent integrals and a change of integration order is performed. Introducing the relative simplex coordinates

$$\begin{aligned} \mu_1 &= \eta_1 - \xi_1 \,, \\ \mu_2 &= \eta_2 - \xi_2 \,, \end{aligned} \tag{11}$$

and replacing into Eq. (10) it results

$$I = \int_0^1 \mathrm{d}\xi_1 \int_{-\xi_1}^{1-\xi_1} \mathrm{d}\mu_1 \int_0^{\xi_1} \mathrm{d}\xi_2 \int_{-\xi_2}^{\mu_1+\xi_1-\xi_2} \mathrm{d}\mu_2 \, f(\boldsymbol{\xi}, \boldsymbol{\mu}) \,, \tag{12}$$

with $\boldsymbol{\xi} = (\xi_1, \xi_2)$ on the p panel and $\boldsymbol{\mu} = (\mu_1, \mu_2)$ on the q one. The natural integration order $(\mu_2, \xi_2, \mu_1, \xi_1)$ is conveniently changed to the $(\xi_2, \xi_1, \mu_2, \mu_1)$ one, and the integrals that have overlapping domains are combined, e.g. see (Taylor, 2003a,b), resulting

$$I = E_1 + E_2 + E_3 + E_4 + E_5 + E_6 \,, \tag{13}$$

	μ_1	μ_2	ξ_1	ξ_2
E_1	$-1 \leq \mu_1 \leq 0$	$\mu_1 \leq \mu_2 \leq 0$	$-\mu_1 \leq \xi_1 \leq 1$	$-\mu_2 \leq \xi_2 \leq \xi_1 + \mu_1 - \mu_2$
E_2	$0 \leq \mu_1 \leq 1$	$0 \leq \mu_2 \leq \mu_1$	$0 \leq \xi_1 \leq 1 - \mu_1$	$0 \leq \xi_2 \leq \xi_1$
E_3	$-1 \leq \mu_1 \leq 0$	$0 \leq \mu_2 \leq 1 + \mu_1$	$\mu_2 - \mu_1 \leq \xi_1 \leq 1$	$0 \leq \xi_2 \leq \xi_1 + \mu_1 - \mu_2$
E_4	$0 \leq \mu_1 \leq 1$	$\mu_1 - 1 \leq \mu_2 \leq 0$	$-\mu_2 \leq \xi_1 \leq 1 - \mu_1$	$-\mu_2 \leq \xi_2 \leq \xi_1$
E_5	$-1 \leq \mu_1 \leq 0$	$-1 \leq \mu_2 \leq \mu_1$	$-\mu_2 \leq \xi_1 \leq 1$	$-\mu_2 \leq \xi_2 \leq \xi_1$
E_6	$0 \leq \mu_1 \leq 1$	$\mu_1 \leq \mu_2 \leq 1$	$\mu_2 - \mu_1 \leq \xi_1 \leq 1 - \mu_1$	$0 \leq \xi_2 \leq \xi_1 + \mu_1 - \mu_2$

Table 1: Integration extremes of the relative μ_1, μ_2 and ξ_1, ξ_2 simplex coordinates for the integrals E_n, for $n = 1, 2, ..., 6$, for contiguous or coincident facets (Taylor, 2003a).
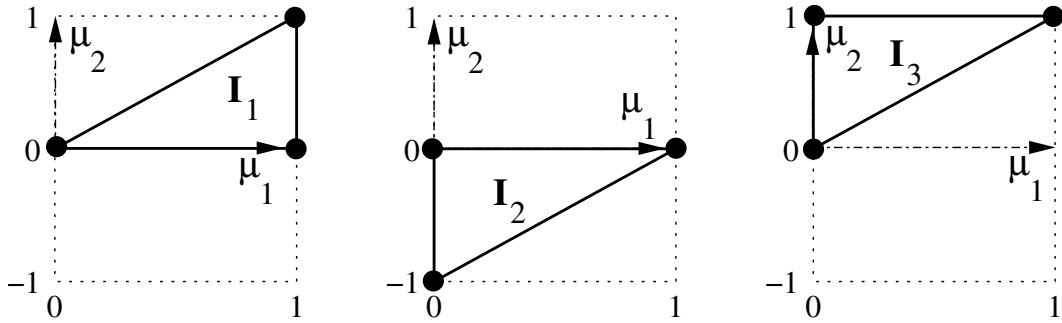
Figure 3: Integration regions for the self–integrals I_1, I_2 and I_3, from left to right, respectively.

where the six integrals E_n have the new integration order

$$E_n = \int \mathrm{d}\mu_1 \int \mathrm{d}\mu_2 \int \mathrm{d}\xi_1 \int \mathrm{d}\xi_2 \, f(\boldsymbol{\xi}, \boldsymbol{\mu}) \,, \qquad (14)$$

for $n = 1, 2, ..., 6$, with the integration extremes listed in Table 1. Thus, the integration region in the plane of the relative coordinates μ_1, μ_2 consists of six triangles with a common vertex at the origin, see Fig. 2.

4 COMMON FACETS

In the case of common facets, Taylor found that the symmetry reduces the six integrals E_n to three ones, i.e.

$$I = I_1 + I_2 + I_3 \,, \qquad (15)$$

with

$$I_n = \int \mathrm{d}\mu_1 \int \mathrm{d}\mu_2 \int \mathrm{d}\xi_1 \int \mathrm{d}\xi_2 \, [f(\boldsymbol{\xi}, \boldsymbol{\eta}) + f(\boldsymbol{\eta}, \boldsymbol{\xi})] \,, \qquad (16)$$

for $n = 1, 2, 3$, where their integration extremes are listed in Table 2. Introducing in Eq. (16) the Duffy coordinate transformations ω, x chosen by Taylor and summarized in Table 3, and the

	μ_1	μ_2	ξ_1	ξ_2
I_1	$0 \leq \mu_1 \leq 1$	$0 \leq \mu_2 \leq \mu_1$	$0 \leq \xi_1 \leq 1 - \mu_1$	$0 \leq \xi_2 \leq \xi_1$
I_2	$0 \leq \mu_1 \leq 1$	$\mu_1 - 1 \leq \mu_2 \leq 0$	$-\mu_2 \leq \xi_1 \leq 1 - \mu_1$	$-\mu_2 \leq \xi_2 \leq \xi_1$
I_3	$0 \leq \mu_1 \leq 1$	$\mu_1 \leq \mu_2 \leq 1$	$\mu_2 - \mu_1 \leq \xi_1 \leq 1 - \mu_1$	$0 \leq \xi_2 \leq \xi_1 + \mu_1 - \mu_2$

Table 2: Integration extremes of the relative μ_1, μ_2 and ξ_1, ξ_2 simplex coordinates for the integrals I_n, for $n = 1, 2, 3$, in the common facet case (Taylor, 2003a).

	I_1	I_2	I_3
μ_1	ω	ωx	ωx
μ_2	ωx	$\omega(x-1)$	ω

Table 3: Duffy coordinate transformations chosen by Taylor in the case of common panels, with $0 \leq \omega, x \leq 1$ (Taylor, 2003a).

	I_1	I_2	I_3
J_n	$(1-\mu_1)\xi_1$	$(1-\mu_1+\mu_2)(\xi_1+\mu_2)$	$(1-\mu_2)(\xi_1-\mu_2+\mu_1)$
ξ_1	$(1-\mu_1)\chi_1$	$(1-\mu_1+\mu_2)\chi_1-\mu_2$	$(1-\mu_2)\chi_1+\mu_2-\mu_1$
ξ_2	$\xi_1\chi_2$	$(\xi_1+\mu_2)\chi_2-\mu_2$	$(\xi_1-\mu_2+\mu_1)\chi_2$

Table 4: Jacobian J_n and integration coordinates ξ_1, ξ_2 as a function of the relative coordinates $0 \leq \mu_1, \mu_2, \chi_1, \chi_2 \leq 1$ in the case of the self–integrals I_1, I_2 and I_3 (Taylor, 2003a).

normalized coordinates χ_1, χ_2 given in Table 4, each integral I_n is regularized and ready for a numerical quadrature using the expression

$$I_n = J_a J_n \int_0^1 \mathrm{d}\omega \int_0^1 \mathrm{d}x \int_0^1 \mathrm{d}\chi_1 \int_0^1 \mathrm{d}\chi_2 \left[f(\boldsymbol{\xi}, \boldsymbol{\eta}) + f(\boldsymbol{\eta}, \boldsymbol{\xi}) \right], \tag{17}$$

for $0 \leq n \leq 3$, where the common Jacobian $J_a = \omega$ is due to the generalized Duffy transformations summarized in Table 3, also see Fig. 3. Each Jacobian J_n comes from the interval maps from $\xi_{1,\mathrm{min}} \leq \xi_1 \leq \xi_{1,\mathrm{max}}$ and $\xi_{2,\mathrm{min}} \leq \xi_2 \leq \xi_{2,\mathrm{max}}$, to the normalized ones $0 \leq \chi_1, \chi_2 \leq 1$, see Table 4. The dependences of the variables ξ_1, ξ_2 with respect to the integration variables $\mu_1, \mu_2, \chi_1, \chi_2$ are summarized in the same Table 4. Note that the variables ξ_1, ξ_2 define the position of one integration point on the considered panel, while the relative coordinates μ_1, μ_2 are defined by the generalized Duffy transformations. The position of the remaining integration point η_1, η_2 on the common panel is known using both coordinates sets and Eq. (11).

5 TWO PANELS WITH A COMMON EDGE

The local numbering scheme of the panel nodes used by Taylor is followed. If two panels share a common edge, then a circular shift in the local numbering of the panel nodes is made in such a way that the common edge has the local vertex numbers 1 and 2 on both simplices. It should be noted that only in this case of common edges, the local numbering of the panel nodes is performed in counterclockwise on the p panel, and clockwise on the q panel, see Fig. 4. Under these conditions, for regularizing each of the integrals E_n, Taylor generalized the Duffy transformations through the expressions summarized in Table 5, where all of them have the same Jacobian $J_b = x_1\omega^2$ and $0 \leq \omega, x_1, x_2 \leq 1$. Due to the several mathematical expressions
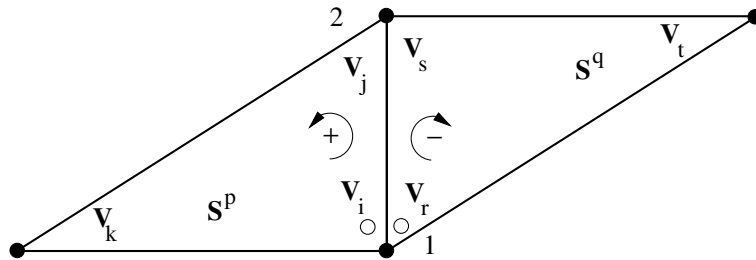
Figure 4: Local numbering scheme of the nodes in the common edge case: counterclockwise on the p panel, and clockwise on the q panel.

involved, it is convenient to put some checks in the computational algorithm, for example, the points (ξ_1, ξ_2) and (η_1, η_2) must always remain in the corresponding simplex domains. As a result of this control, for instance, a sign discrepancy in the second entry of the E_4 column was found with respect to the original version of Taylor (Taylor, 2003a). Taking each integral E_n

	E_1	E_2	E_3	E_4	E_5	E_6
μ_1	$-\omega x_1$	ωx_1	$-\omega x_1 x_2$	$\omega x_1 x_2$	$-\omega x_1 x_2$	$\omega x_1 x_2$
μ_2	$-\omega x_1 x_2$	$\omega x_1 x_2$	$\omega x_1(1 - x_2)$	$\omega x_1(x_2 - 1)$	$-\omega x_1$	ωx_1

Table 5: Duffy transformations used by Taylor for each one of the six integrals when the common edge is defined by the vertex $\mathbf{V}_1$ and $\mathbf{V}_2$, where $0 \leq \omega, x_1, x_2 \leq 1$. Note: there is a sign discrepancy in the second entry of the E_4 column with respects to the original one given in (Taylor, 2003a).

separately and performing some algebra (e.g. see Appendix), all these integrals are regularized. The common final expressions are given by

$$E_n = J_b \tilde{J} \int_0^1 \mathrm{d}\omega \int_0^1 \mathrm{d}x_1 \int_0^1 \mathrm{d}x_2 \int_0^1 \mathrm{d}\chi_1 \, (...) , \qquad (18)$$

for $0 \leq n \leq 6$, where the Jacobian $J_b = x_1 \omega^2$ is due to the generalized Duffy transformation, while $\tilde{J} = 1 - \omega$ is originated by the mapping from the interval $\xi_{1,\min} \leq \xi_1 \leq \xi_{1,\max}$ to the normalized $0 \leq \chi_1 \leq 1$ one. The functional dependences of the simplex coordinates ξ_1, ξ_2 with respect to the integration ones (ω, x_1, x_2, χ) in each E_n integral are summarized in Table 6.
In summary, first, the quadrature point $\mathbf{x}(\xi_1, \xi_2)$ on the p panel is computed through Table 6; next, the relative simplex coordinates μ_1, μ_2 are obtained by the generalized Duffy transformations ω, x_1, x_2 given in Table 5; and finally, the quadrature point $\mathbf{y}(\eta_1, \eta_2)$ on the q panel is computed using Eq. (11).

	ξ_1	ξ_2
E_1	$(1-\omega)\chi_1 + \omega$	$\omega(1 - x_1 + x_1 x_2)$
E_2	$(1-\omega)\chi_1 + \omega(1 - x_1)$	$\omega(1 - x_1)$
E_3	$(1-\omega)\chi_1 + \omega$	$\omega(1 - x_1)$
E_4	$(1-\omega)\chi_1 + \omega(1 - x_1 x_2)$	$\omega(1 - x_1 x_2)$
E_5	$(1-\omega)\chi_1 + \omega$	ω
E_6	$(1-\omega)\chi_1 + \omega(1 - x_1 x_2)$	$\omega(1 - x_1)$

Table 6: Simplex coordinates ξ_1, ξ_2 as a function of the quadrature ones ω, x_1, x_2, χ_1, for the integrals E_n, for $n = 1, 2, ..., 6$ in the case of a common edge with local vertex $\mathbf{V}_1$ and $\mathbf{V}_2$, where $0 \leq \omega, \chi_1, x_1, x_2 \leq 1$.

6 COMMON VERTEX

If two panels share a vertex, a permutation on the local numbering of the panel nodes is performed in such a way that the common vertex has the local vertex number 1 on each panel. In this case, the distance

$$r = \mathbf{x} - \mathbf{y} = (\eta_1 - \xi_1)\mathbf{V}_1 + (\xi_1 - \xi_2)\mathbf{V}_2 + \xi_2 \mathbf{V}_3 - (\eta_1 - \xi_1)\mathbf{V}_2' - \eta_2 \mathbf{V}_3' , \qquad (19)$$

is null since $\xi_1 = \xi_2 = \eta_1 = \eta_2 = 0$ which is the origin of the simplex coordinate system in four dimensions (in 4D). In this case, the Taylor strategy begins with the integral

$$I = \int_0^1 \mathrm{d}\xi_1 \int_0^{\xi_1} \mathrm{d}\xi_2 \int_0^1 \mathrm{d}\eta_1 \int_0^{\eta_1} \mathrm{d}\eta_2 \, f(\boldsymbol{\xi}, \boldsymbol{\eta}) , \qquad (20)$$

whose integration domain is re-written as

$$I = \int_0^1 d\xi_1 \int_0^{\xi_1} d\eta_1 \int_0^{\xi_1} d\xi_2 \int_0^{\eta_1} d\eta_2 \left[f(\boldsymbol{\xi}, \boldsymbol{\eta}) + f(\boldsymbol{\eta}, \boldsymbol{\xi}) \right], \tag{21}$$

which has an isolated singularity at the origin and is directly regularized with a Duffy coordinate transformation in four dimensions and summarized in Table 7, giving

$$I = J_c \int_0^1 d\omega \int_0^1 dz_1 \int_0^1 dz_2 \int_0^1 dz_3 \left[f(\boldsymbol{\xi}, \boldsymbol{\eta}) + f(\boldsymbol{\eta}, \boldsymbol{\xi}) \right], \tag{22}$$

with the Jacobian $J_c = z_2 \omega^3$.

coordinates	after a Duffy transformation
(ξ_1, ξ_2)	$(\omega, \omega z_1)$
(η_1, η_2)	$(\omega z_2, \omega z_2 z_3)$

Table 7: Duffy coordinate transformation in the four dimensional space when both panels share the vertex $\mathbf{V}_1$.

7   NUMERICAL TESTS

Four numerical tests are considered in the following sections: a triangular domain, a square domain, a refined square domain, and a comparison between irregular tessellations of the square domain with triangles and quadrilaterals. In each case, the proposed scheme and the Wang-Atalla approach are employed over triangles and quadrilaterals, respectively, for computing double surface integrals and comparing the numerical results against the corresponding analytical solutions.

Regarding to the computational cost, it can be said that both methods, full modified Taylor and Wang–Atalla, require a similar number of operations. On one hand, the Wang–Atalla scheme with n_{1d} integration points in each coordinate involves a first stage where the full table of integration points must be built, a task typically with $O(n_{1d}^2)$ operations of symmetry that can be made as a preprocessing stage. Next, the numerical quadrature is performed through a nested double loop p, q for computing the matrix entries Z_m^{pq}, giving $O(n_{1d}^4)$ operations by pair of interacting elements. Since there are $E \times E$ pairs of interacting elements, then a total of $O(E^2 n_{1d}^4)$ operations are performed for each integral Z_m. On the other hand, the present approach involves a previous preprocessing stage where all the pairs of interaction elements are classified as (a) self–influence, (b) with an edge singularity, (c) with a vertex singularity, or (d) regulars, i.e. those that have neither edge nor vertex in common. In cases b-c, a circular shift in the nodes numbering of the neighbouring elements is performed to obtain the corresponding ones assumed by the Taylor algorithm. All this information can be stored in an auxiliary array $D(E, n_{\text{neighbour}}, n_{\text{m}})$, of rank 3, where $n_{\text{neighbour}}$ is the maximum number of panel neighbours of each panel at its first layer, while the third index stores other useful data (with $n_{\text{m}} = 4$ in the present implementation). Then, there is a total of $O(E^2 n_{1d}^4)$ operations for each integral Z_m.

7.1   Triangular domain

In the first numerical test, the following integral is computed:

$$\hat{Z}_0 = \int_{-1}^{+1} d\alpha \int_{-1}^{+1} d\beta \int_{-1}^{+1} d\gamma \int_{-1}^{+1} d\delta \, \frac{1}{r}, \tag{23}$$
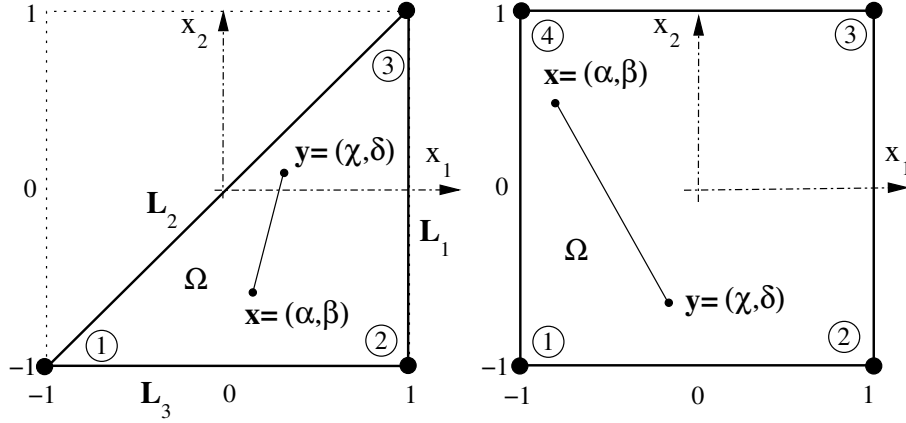
Figure 5: Triangular and square integration domains Ω, with side length $L = 2$, used in the tests. The Wang–Atalla integration was used on the square domain for the double surface integral of h_m/r, where $r = \|\mathbf{x} - \mathbf{y}\|_2$, with $\mathbf{x}, \mathbf{y} \in \Omega$. The regular multiplicative functions h_m are detailed in Table 9.

where the integration domain Ω is the flat triangle of side length $L = 2$ shown in Fig. 5 (left), and $r = \|\mathbf{x} - \mathbf{y}\|_2$ is the Euclidean distance between the integration points $\mathbf{x} = (\alpha, \beta)$ and $\mathbf{y} = (\gamma, \delta)$, respectively. The numerical values obtained for Eq. (23) are shown in Table 8

n_{1d}	collapsed WA	$\varepsilon_r\%$	modified Taylor	$\varepsilon_r\%$
2	7.542 123	-6.01	7.968 865	-0.69
3	7.557 045	-5.82	8.032 884	0.10
4	7.882 916	-1.76	8.023 229	-0.01
semi-analytical			8.024 527	

Table 8: Numerical evaluation of Eq. (23) using n_{1d} integration points in each coordinate: values obtained with the Wang–Atalla (WA) scheme with the fourth side collapsed (2nd column), and those with the present approach (3rd column).

using $n_{1d} = 2, 3, 4$ integration points in each coordinate for the Wang–Atalla scheme (2nd column), and for the proposed modified Taylor (3rd column). The first method is applied on the triangular domain by collapsing one side of the square. The Wang–Atalla formulae are partially listed in Tables I-IV of their paper (Wang and Atalla, 1997) for a practical use, because there are symmetries both in the weights functions and in the integration points. Nevertheless, it should be noted that these symmetries are not trivial to write in full in some cases since there are four integration coordinates. The exact value for $\hat{Z}_0$ is computed using the expression given by Sievers *et al.* (Eibert and Hansen, 1995; Sievers et al., 2005)

$$\hat{Z}_0 = \frac{1}{3L_1}\ln_1 + \frac{1}{3L_2}\ln_2 + \frac{1}{3L_3}\ln_3 \,, \tag{24}$$
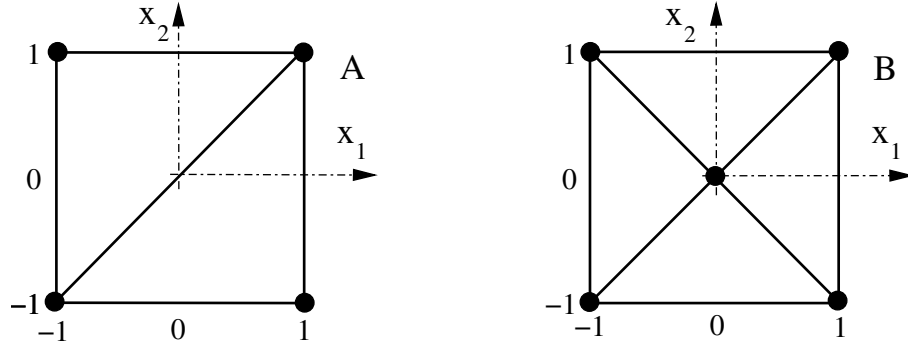
Figure 6: Two partitions $O(L)$ of the square of length side $L = 2$ with linear triangles: mesh A with edge singularities only (left), and mesh B with vertex and edge singularities (right), for the example of Sec. 7.2.

where $L_1 = \|\mathbf{x}_2 - \mathbf{x}_3\|_2$, $L_2 = \|\mathbf{x}_3 - \mathbf{x}_1\|_2$ and $L_3 = \|\mathbf{x}_1 - \mathbf{x}_2\|_2$ are the lengths of the triangle sides, and

$$\ln_1 = \ln\left|\frac{(L_1 + L_2)^2 - L_3^2}{L_2^2 - (L_3 - L_1)^2}\right|, \tag{25}$$

$$\ln_2 = \ln\left|\frac{(L_2 + L_3)^2 - L_1^2}{L_3^2 - (L_1 - L_2)^2}\right|, \tag{26}$$

$$\ln_3 = \ln\left|\frac{(L_3 + L_1)^2 - L_2^2}{L_1^2 - (L_2 - L_3)^2}\right|. \tag{27}$$

7.2 Square domain

This numerical test is inspired from the one presented by W. Wang and N. Atalla (Wang and Atalla, 1997), where the following integral is computed:

$$Z_m = \int_{-1}^{+1} d\alpha \int_{-1}^{+1} d\beta \int_{-1}^{+1} d\gamma \int_{-1}^{+1} d\delta \frac{h_m}{r}, \tag{28}$$

where the integration domain Ω is the flat square of side length $L = 2$, centered at the origin, see Fig. 5 (right), $r = \|\mathbf{x} - \mathbf{y}\|_2$ is the Euclidean distance between the integration points $\mathbf{x} = (\alpha, \beta)$ and $\mathbf{y} = (\gamma, \delta)$, respectively, and $h_m = h_m(\alpha, \beta, \gamma, \delta)$ are the regular multiplicative test functions summarized in Table 9. The square domain Ω is split into E triangle subdomains

m	h_m	semi-analytical Z_m
0	1	23.785677
1	$\alpha\beta\gamma\delta$	0.705130
2	$(\alpha\beta\gamma\delta)^2$	0.337057
3	$(\alpha\beta\gamma\delta)^3$	0.083744
4	$(\alpha\beta\gamma\delta)^4$	0.057834

Table 9: Square domain test: regular functions h_m (2nd column), and semi-analytical Z_m values with 6 digits accuracy (3rd column), as reported by Wang–Atalla (Wang and Atalla, 1997).
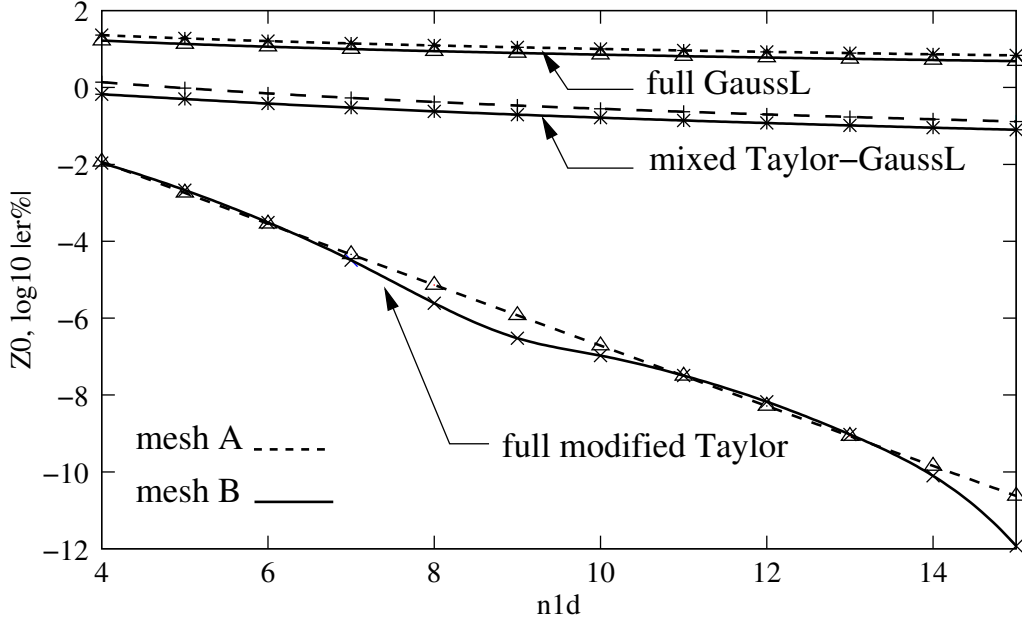
Figure 7: Absolute value of the relative percent error $|e_r\%|$ of the Z_0 integral with respect to the number of the integration points in each coordinate n_{1d}: (i) full modified Taylor; (ii) mixed modified Taylor and GaussL, with the modified Taylor scheme in the self–integral only, and the Gauss–Legendre one otherwise; and (iii) full GaussL, with the Gauss-Legendre scheme in all the domain ignoring the singularities, using the meshes A and B in Fig. 6.

Ω^p such that

$$\Omega = \cup\Omega^p \quad \text{for } p = 1, 2, ..., E;$$
$$\Omega^p \cap \Omega^q = \emptyset \quad \text{with } p \neq q;$$

(29)

therefore

$$Z_m = \sum_{p,q=1}^{E} Z_m^{pq} ,$$

(30)

where

$$Z_m^{pq} = \int_{\Omega^p} \mathrm{d}\Omega^p \int_{\Omega^q} \mathrm{d}\Omega^q \, \frac{h_m}{r} \quad , \quad 1 \leq p, q \leq E .$$

(31)

Two simple partitions $O(L)$ of the square are shown in Fig. 6: mesh A consists of two triangles that share a common edge, arising an edge singularity (left), and mesh B has four triangles sharing edges and a vertex at the origin, arising edge and vertex singularities, respectively (right). Equation (28) is computed with the regular test functions h_m listed in the second column of Table 9, while the semi-analytical Z_m values are listed in the third column. These coefficients can be calculated through recurrence relations developed by Berry (Berry, 1994). The exact value for Z_0 is computed using (Wang and Atalla, 1997)

$$Z_0 = 16 \left[\ln \frac{\sqrt{2} + 1}{\sqrt{2} - 1} - \frac{2}{3}(1 - \sqrt{2}) \right] .$$

(32)

Results are displayed for computations done with a variable number of integration points in each coordinate, always with smooth asymptotic convergence. The integration points were computed using an algorithm given by Quarteroni *et al.* (Quarteroni et al., 2000). In Figs. 7-9, a comparison is shown among: (i) full modified Taylor; (ii) mixed modified Taylor and GaussL, with the modified Taylor scheme used in the self–integral only, and the Gauss–Legendre one
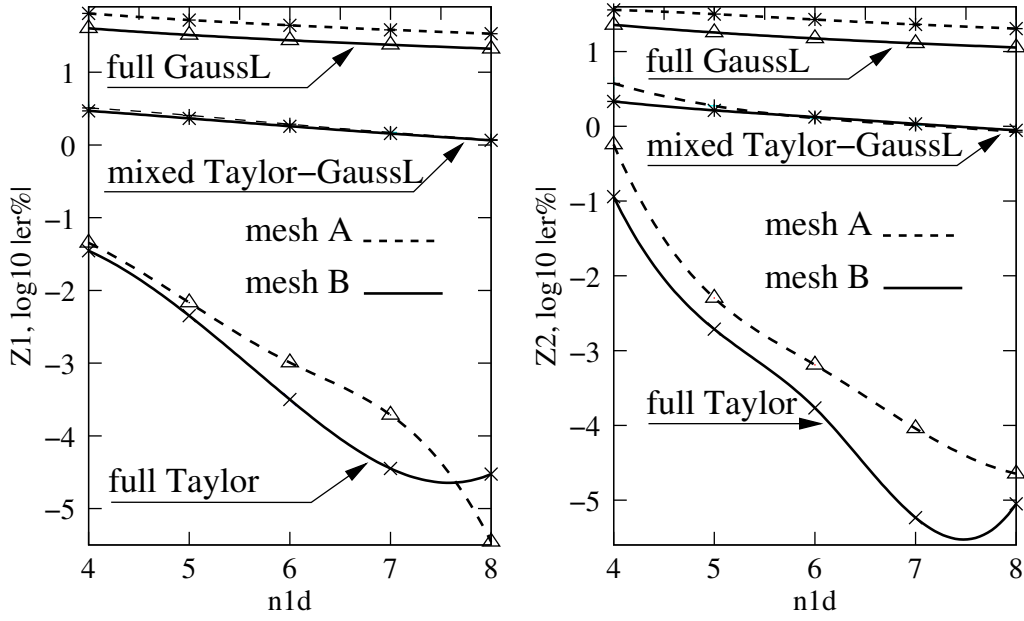
Figure 8: Idem Fig. 7 for Z_1 (left) and Z_2 (right).

otherwise; and (iii) full GaussL, with the Gauss-Legendre scheme in all the domain ignoring the singularities. The relative percent error $e_r\%$ is computed with

$$e_r\%(Z_m) = \frac{Z_{m,\text{num}} - Z_{m,\text{semi-analytical}}}{Z_{m,\text{semi-analytical}}} \times 100 \; ; \tag{33}$$

for $0 \leq m \leq 4$, and plotted with respect to the number of the integration points in each coordinate n_{1d} in semi-logarithmic scale. It can be seen that both, the numerical scheme with a special formula for the self–integral only, and the Gauss–Legendre quadrature formula that neglects the edge, vertex and self–influence singularities, introduce a relative error which is several orders of magnitude larger than the present approach in almost cases. Furthermore, additional checks can be performed verifying the symmetry properties (Berry, 1994)

$$Z_{mnpq} = 0 \quad \text{when } (m + p) \text{ is odd or } (n + q) \text{ is odd,} \tag{34}$$

$$Z_{mnpq} = Z_{pnmq} = Z_{mqpn} = Z_{pqmn} \; . \tag{35}$$

n_{1d}	scheme	Z_0	Z_1	Z_2	Z_3	Z_4
2	Taylor	-4.36×10^{-2}	-1.92	-7.17	-29.30	-44.64
	WA	-7.04×10^{-1}	-9.56×10^{-1}	-4.02	-26.37	-38.76
3	Taylor	$+2.29 \times 10^{-2}$	$+1.37 \times 10^{-1}$	-2.55×10^{-1}	-2.30	-5.97
	WA	-3.91	-8.26	-1.08	-6.52×10^{-1}	-2.63
4	Taylor	-1.14×10^{-2}	-2.32×10^{-2}	-2.14×10^{-2}	-2.22×10^{-1}	-6.29×10^{-1}
	WA	$+8.83 \times 10^{-2}$	-1.43×10^{-2}	-5.03×10^{-4}	$+1.37 \times 10^{-4}$	-1.93×10^{-1}

Table 10: Relative percent error $e_r\%$ for the Z_0-Z_4 integrals, with respect to the number of the integration points in each coordinate n_{1d}, obtained with the modified Taylor integration on triangles and the Wang–Atalla (WA) one on quadrilaterals, using the uniform refined mesh C of Fig. 10.
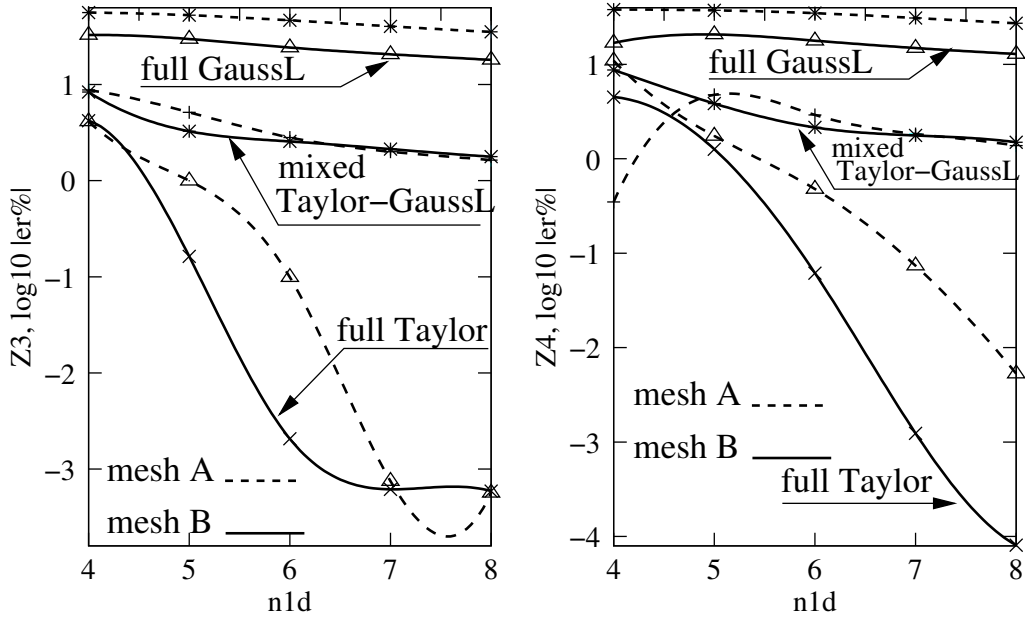
Figure 9: Idem Fig. 7 for Z_3 (left) and Z_4 (right).
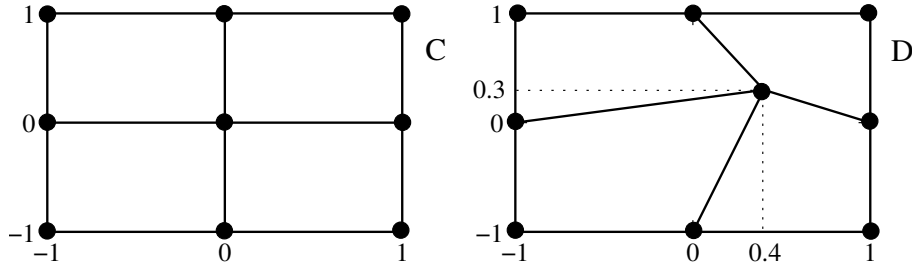
Figure 10: A refined square domain of length side $L = 2$ with a uniform mesh C (left), and with a perturbed one D (right).

n_{1d}	scheme	Z_0	Z_1	Z_2	Z_3	Z_4
2	Taylor	$+2.13 \times 10^{-2}$	$+3.85 \times 10^{-1}$	-4.80	-26.12	-41.22
	WA	-0.99	-2.67	-4.59	-26.85	-38.87
3	Taylor	-3.28×10^{-2}	$+2.91 \times 10^{-2}$	$+3.85 \times 10^{-1}$	-1.13×10^{-1}	-3.46
	WA	-3.90	-8.06	-1.37	-1.01	-2.84
4	Taylor	1.32×10^{-2}	$+7.27 \times 10^{-3}$	$+3.82 \times 10^{-2}$	$+3.59 \times 10^{-1}$	$+3.49 \times 10^{-1}$
	WA	7.00×10^{-2}	-4.26×10^{-1}	-1.43×10^{-1}	-6.88×10^{-2}	-2.08×10^{-1}

Table 11: Idem Table 10 using the perturbed refined mesh D of Fig. 10.

7.3 Refined square domain

A refined square domain of side length $L = 2$ is tested, with both a uniform and a perturbed mesh, as is shown in Fig. 10. A comparison of results is given in Tables 10-11 between the proposed scheme on triangles, and the Wang–Atalla one on quadrilaterals, for the relative percent error $e_r\%$ in the values, from Z_0 to Z_4. Figures 11-12 show convergence plots of the absolute relative percent error $|e_r\%|$ with respect to the number of the integration points in each coordinate n_{1d} with the proposed method. From these results, it can be seen that the proposed scheme leads to relative percent errors which are several orders of magnitude smaller than the Wang–
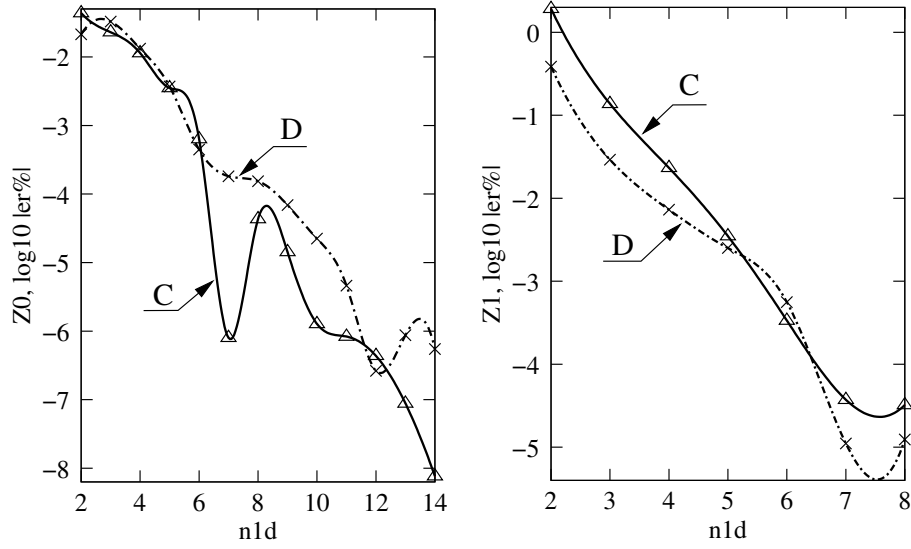
Figure 11: Convergence of the absolute relative percent error $|e_r\%|$ with respect to the number of the integration points in each coordinate n_{1d} with the proposed method using the refined meshes C and D of Fig. 10. Integrals Z_0 (left) and Z_1 (right).
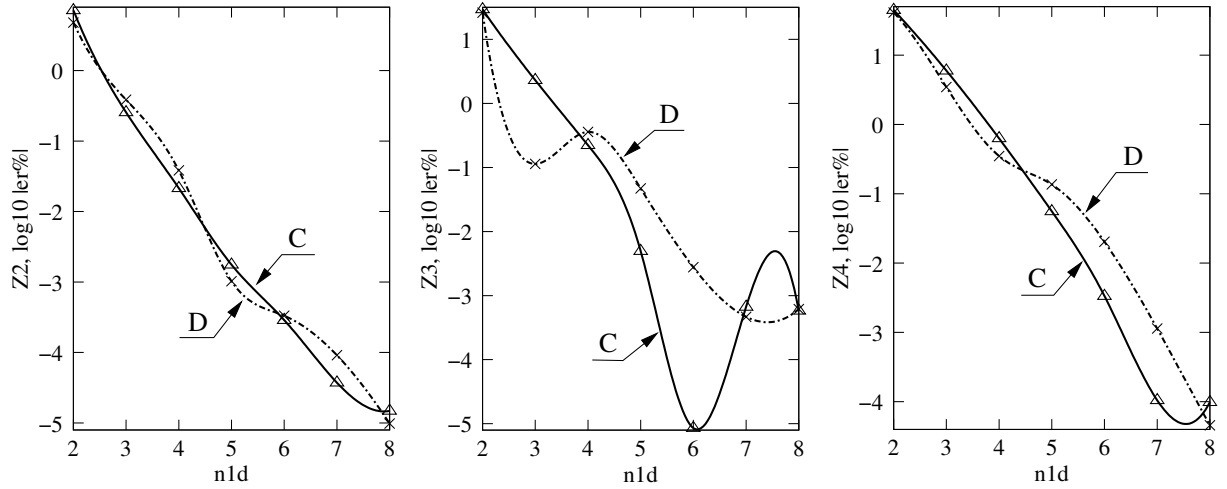
Figure 12: Idem Fig. 11 for integral Z_2 (left), Z_3 (centre) and Z_4 (right).

Atalla one, when the number of the integration points in each coordinate n_{1d} is increased. This can be attributed to the fact that the present approach takes into account the common edge and vertex singularities, which are neglected in the Wang–Atalla scheme. Only the self–integral is computed with a special formula in the Wang–Atalla scheme, while a Gauss–Legendre rule is used for the remaining pairs of interacting panels.

7.4 Irregular tessellations with triangles and quadrilaterals

In this section, Eq. (28) and Table 9 are again computed on the same flat square Ω of side length $L = 2$, centered at the origin, as is shown in Fig. 5 (right). First, four tessellations with quadrilaterals are used and, next, these quadrilaterals are subdivided into triangles. Thus, in Fig. 13, the square Ω is partitioned in the meshes E-H with quadrilaterals (solid lines), and triangles (dashed lines). Plots of the convergence of the relative percent error $|e_r\%|$ of the value of Z_m with respect to the number of the integration points in each coordinate n_{1d} are shown in Figs.
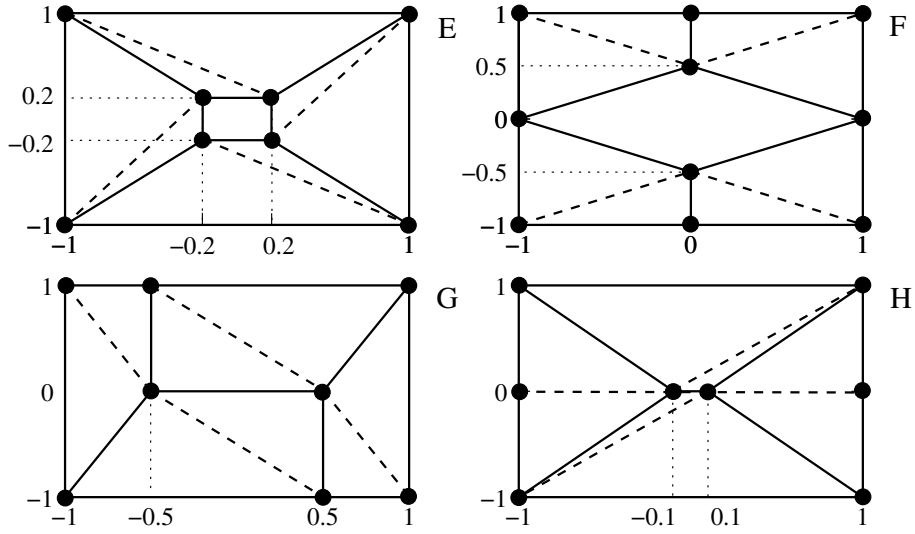
Figure 13: Irregular tessellations of the square of length side $L = 2$ with the meshes E-H using: quadrilaterals (solid lines) and triangles (dashed lines).

14-15, for the integrals from Z_0 to Z_4, respectively, with the proposed scheme over triangles (curves E-H). Results with the Wang-Atalla scheme over quadrilaterals are not included due to length limitations, although they show a same behaviour as those of the previous section.

8 CONCLUSIONS

In this work a modified Taylor scheme (Taylor, 2003a) for computing the singular surface integrals encountered in Galerkin boundary element methods has been presented. The scheme is oriented to flat triangles, and removes the weak singularities in the integrand through a series of coordinate transformations, coupled with an interchange of the order of integration followed by appropriate Duffy coordinate transformations. It allows to take into account the field singularity due to the self–influence, edge and vertex singularities, and it can be employed as a "black box" in practical applications. Contrary to the original version, the present strategy consists in a full numerical quadrature scheme in the four simplex coordinates and is not specialized for any particular kernel. The extremes of the ξ_1, ξ_2 integrals, when two panels have a common edge, are given by the six entries E_n in Table 6 that are neither presented nor discussed by Taylor in (Taylor, 2003a), although they are necessary when a full numerical quadrature is chosen in the four simplex coordinates. Four types of numerical tests were considered: a triangular domain, a square domain, a refined square domain, and a comparison between irregular tessellations of a square domain with triangles and quadrilaterals. In each case, the proposed scheme and the Wang-Atalla approach were employed over triangles and quadrilaterals, respectively, to compute double surface integrals. The numerical results obtained with the proposed method in all cases compare favorably with those obtained with the Wang–Atalla scheme. The square domain test was designed for evaluating the overall performance of the numerical schemes in the cases: (a) self–influence and edge singularity; (b) self—influence, edge and vertex singularity; and (c) self–influence neglecting the edge and vertex singularities. In all cases, the proposed method showed higher accuracy and better convergence properties than more classical ideas, for instance, the use of a special scheme for handling self–integral together with a Gauss–Legendre integration for the remaining interactions. The convergence plots shown that proposed scheme leads to relative percent errors which are several orders of magnitude smaller than the Wang–
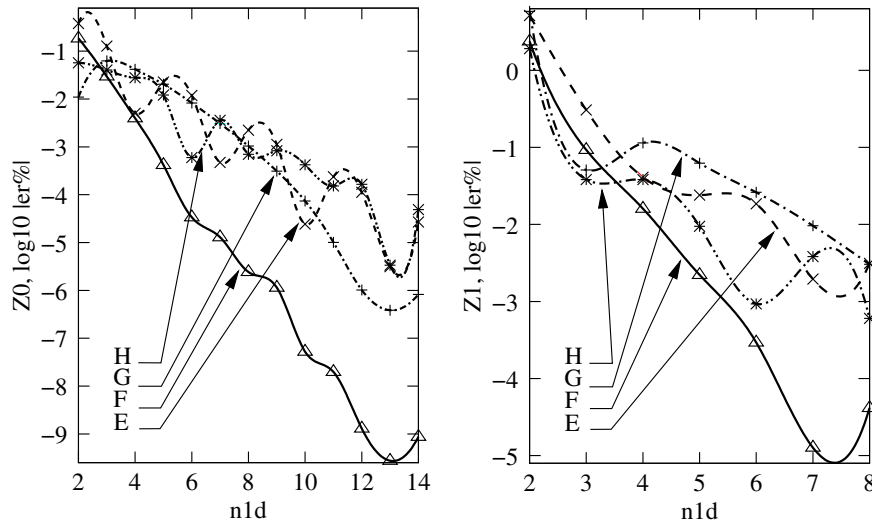
Figure 14: Convergence of the absolute relative percent error $|e_r\%|$ with respect to the number of the integration points in each coordinate n_{1d} with the proposed method using the irregular meshes E-H of Fig. 13. Integrals Z_0 (left) and Z_1 (right).
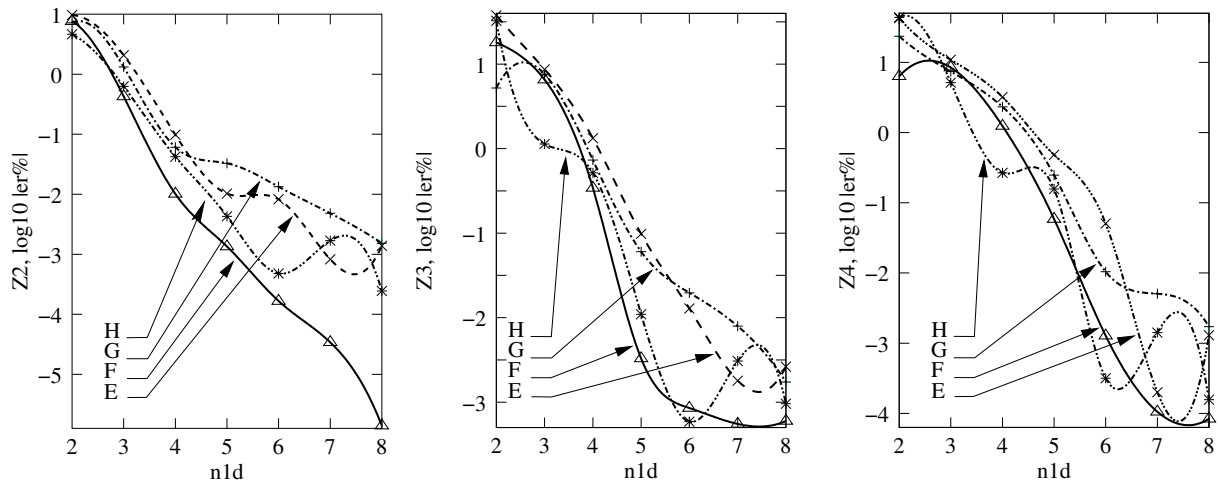
Figure 15: Idem Fig. 14 for integral Z_2 (left), Z_3 (centre) and Z_4 (right).

Atalla one when the number of the integration points in each coordinate n_{1d} is increased. The numerical results show that although the Wang–Atalla approach is a natural choice for the self–integrals in quadrilateral elements, its performance is deteriorated when a mesh refinement is performed, that can be attributed to the fact of ignoring the contributions of edge and vertex singularities. Moreover, although the Wang–Atalla formulae could be employed for use on triangles by means of the collapse of one side of the quadrilateral element, such strategy will inevitably introduce, first, a bias on the integral value due to the lack of invariance against the numbering of the local nodes and, second, a larger relative percent error than the one found with the proposed methodology. For these reasons, the modified Taylor methodology proposed in this paper could be preferable to the Wang-Atalla one when a more precise numerical integration scheme might be chosen for triangles. Further development could be focused on the extension of the modified Taylor strategy to other types of finite elements, as the quadrilateral case.

Acknowledgments

9   APPENDIX

In this appendix, the coordinate transformations for the common edge case that were not detailed in (Taylor, 2003a) are summarized. It should be noted that in Eqns. (42, 48, 55, 62, 69, 75):

i) The auxiliary coordinate s_2 which is introduced in the following equations is later identified as the integration variable ω, that is, $s_2 \equiv \omega$;

ii) The last mapping from the $s_2 \leq \xi_1 \leq 1$ interval to the unit one $0 \leq \chi_1 \leq 1$ produces the same additional Jacobian $\tilde{J} = 1 - \omega$ introduced in Eq. (18).

9.1   Integral E_1

Beginning with

$$E_1 = \int_{-1}^{0} d\mu_1 \int_{\mu_1}^{0} d\mu_2 \int_{-\mu_1}^{1} d\xi_1 \int_{-\mu_2}^{\xi_1 + \mu_1 - \mu_2} d\xi_2 \, (...) \,, \tag{36}$$

introducing the auxiliary coordinates $z_1 = -\mu_1$ and $z_2 = -\mu_2$,

$$E_1 = \int_{0}^{1} dz_1 \int_{0}^{z_1} dz_2 \int_{z_1}^{1} d\xi_1 \int_{z_2}^{\xi_1 + z_2 - z_1} d\xi_2 \, (...) \,, \tag{37}$$

interchanging the integration order,

$$\int_{z_1}^{1} d\xi_1 \int_{z_2}^{\xi_1 + z_2 - z_1} d\xi_2 \, (...) = \int_{z_2}^{1 + z_2 - z_1} d\xi_2 \int_{\xi_2 + z_1 - z_2}^{1} d\xi_1 \, (...) \,, \tag{38}$$

introducing the auxiliary coordinate $s_2 = \xi_2 + z_1 - z_2$,

$$\int_{z_2}^{1 + z_2 - z_1} d\xi_2 \int_{\xi_2 + z_1 - z_2}^{1} d\xi_1 \, (...) = \int_{z_1}^{1} ds_2 \int_{s_2}^{1} d\xi_1 \, (...) \,, \tag{39}$$

replacing,

$$E_1 = \int_{0}^{1} dz_1 \int_{0}^{z_1} dz_2 \int_{z_1}^{1} ds_2 \int_{s_2}^{1} d\xi_1 \, (...) \,, \tag{40}$$

where the integration in the z_1, z_2, s_2 coordinates gives the volume of a tetrahedron, then, performing a cyclic permutation,

$$E_1 = \int_{0}^{1} ds_2 \int_{0}^{s_2} dz_1 \int_{0}^{z_1} dz_2 \int_{s_2}^{1} d\xi_1 \, (...) \,, \tag{41}$$

and using the first Duffy transformation of Table 6 corresponding to the E_1 integral, it results

$$E_1 = J_b \int_0^1 d\omega \int_0^1 dx_1 \int_0^1 dx_2 \int_\omega^1 d\xi_1 \, (...) \, . \tag{42}$$

Finally, introducing the linear mapping from the interval $\omega \leq \xi_1 \leq 1$ to the $0 \leq \chi_1 \leq 1$ one, the dependences expressed by the first row of Table 6 are obtained.

9.2 Integral E_2

Beginning with

$$E_2 = \int_0^1 d\mu_1 \int_0^{\mu_1} d\mu_2 \int_0^{1-\mu_1} d\xi_1 \int_0^{\xi_1} d\xi_2 \, (...) \, , \tag{43}$$

interchanging the integration order,

$$\int_0^{1-\mu_1} d\xi_1 \int_0^{\xi_1} d\xi_2 = \int_0^{1-\mu_1} d\xi_2 \int_{\xi_2}^{1-\mu_1} d\xi_1 \, (...) \, , \tag{44}$$

introducing the auxiliary coordinate $s_2 = \xi_2 + \mu_1$,

$$\int_0^{1-\mu_1} d\xi_2 \int_{\xi_2}^{1-\mu_1} d\xi_1 \, (...) = \int_{\mu_1}^1 ds_2 \int_{s_2-\mu_1}^{1-\mu_1} d\xi_1 \, (...) \, , \tag{45}$$

replacing,

$$E_2 = \int_0^1 d\mu_1 \int_0^{\mu_1} d\mu_2 \int_{\mu_1}^1 ds_2 \int_{s_2-\mu_1}^{1-\mu_1} d\xi_1 \, (...) \, , \tag{46}$$

where the integration in the μ_1, μ_2, s_2 coordinates gives the volume of a tetrahedron, then, performing a cyclic permutation,

$$E_2 = \int_0^1 ds_2 \int_0^{s_2} d\mu_1 \int_0^{\mu_1} d\mu_2 \int_{s_2-\mu_1}^{1-\mu_1} d\xi_1 \, (...) \, , \tag{47}$$

and using the second Duffy transformation of Table 6 corresponding to the E_2 integral, it results

$$E_2 = J_b \int_0^1 d\omega \int_0^1 dx_1 \int_0^1 dx_2 \int_0^{s_2-\mu_1} d\xi_1 \, (...) \, . \tag{48}$$

Then, introducing the linear mapping from the interval $0 \leq \xi_1 \leq s_2 - \mu_1$ to the $0 \leq \chi_1 \leq 1$ one, the dependences expressed by the second row of Table 6 are obtained.

9.3 Integral E_3

Starting from

$$E_3 = \int_{-1}^0 d\mu_1 \int_0^{1+\mu_1} d\mu_2 \int_{\mu_2-\mu_2}^1 d\xi_1 \int_0^{\xi_1+\mu_1-\mu_2} d\xi_2 \, (...) \, , \tag{49}$$

introducing the auxiliary coordinate $z_1 = -\mu_1$,

$$E_3 = \int_0^1 dz_1 \int_0^{1-z_1} d\mu_2 \int_{\mu_2+z_1}^1 d\xi_1 \int_0^{\xi_1-z_1-\mu_2} d\xi_2 \, (...) \, , \tag{50}$$

interchanging the integration order,

$$\int_{\mu_2+z_1}^{1} \mathrm{d}\xi_1 \int_{0}^{\xi_1-z_1-\mu_2} \mathrm{d}\xi_2 \, (...) = \int_{0}^{1-z_1-\mu_2} \mathrm{d}\xi_2 \int_{\xi_2+z_1+\mu_2}^{1} \mathrm{d}\xi_1 \, (...) \, , \tag{51}$$

introducing the auxiliary coordinate $s_2 = \xi_2 + z_1 + \mu_2$,

$$\int_{0}^{1-z_1-\mu_2} \mathrm{d}\xi_2 \int_{\xi_2+z_1+\mu_2}^{1} \mathrm{d}\xi_1 \, (...) = \int_{z_1+\mu_2}^{1} \mathrm{d}s_2 \int_{s_2}^{1} \mathrm{d}\xi_1 \, (...) \, , \tag{52}$$

replacing,

$$E_3 = \int_{0}^{1} \mathrm{d}z_1 \int_{0}^{1-z_1} \mathrm{d}\mu_2 \int_{z_1+\mu_2}^{1} \mathrm{d}s_2 \int_{s_2}^{1} \mathrm{d}\xi_1 \, (...) \, , \tag{53}$$

where the integration in the z_1, μ_2, s_2 coordinates gives the volume of a tetrahedron, after performing a cyclic permutation,

$$E_3 = \int_{0}^{1} \mathrm{d}s_2 \int_{0}^{s_2} \mathrm{d}z_1 \int_{0}^{s_2-z_1} \mathrm{d}\mu_2 \int_{s_2}^{1} \mathrm{d}\xi_1 \, (...) \, , \tag{54}$$

and using the third Duffy transformation of Table 6 corresponding to the E_3 integral, it results

$$E_3 = J_b \int_{0}^{1} \mathrm{d}\omega \int_{0}^{1} \mathrm{d}x_1 \int_{0}^{1} \mathrm{d}x_2 \int_{\omega}^{1} \mathrm{d}\xi_1 \, (...) \, . \tag{55}$$

Introducing the linear mapping from the interval $\omega \leq \xi_1 \leq 1$ to the $0 \leq \chi_1 \leq 1$ one, the dependences expressed by the third row of Table 6 are obtained.

9.4 Integral E_4

Beginning with

$$E_4 = \int_{0}^{1} \mathrm{d}\mu_1 \int_{\mu_1-1}^{0} \mathrm{d}\mu_2 \int_{-\mu_2}^{1-\mu_1} \mathrm{d}\xi_1 \int_{-\mu_2}^{\xi_1} \mathrm{d}\xi_2 \, (...) \, , \tag{56}$$

introducing the auxiliary coordinate $z_2 = -\mu_2$,

$$E_4 = \int_{0}^{1} \mathrm{d}z_1 \int_{0}^{1-\mu_1} \mathrm{d}z_2 \int_{z_2}^{1-\mu_1} \mathrm{d}\xi_1 \int_{z_2}^{\xi_1} \mathrm{d}\xi_2 \, (...) \, , \tag{57}$$

interchanging the integration order,

$$\int_{z_2}^{1-\mu_1} \mathrm{d}\xi_1 \int_{z_2}^{\xi_1} \mathrm{d}\xi_2 = \int_{z_2}^{1-\mu_1} \mathrm{d}\xi_2 \int_{\xi_2}^{1-\mu_1} \mathrm{d}\xi_1 \, , \tag{58}$$

introducing the auxiliary coordinate $s_2 = \xi_2 + \mu_1$,

$$\int_{z_2}^{1-\mu_1} \mathrm{d}\xi_2 \int_{\xi_2}^{1-\mu_1} \mathrm{d}\xi_1 = \int_{\mu_1+z_2}^{1} \mathrm{d}\xi_2 \int_{s_2-\mu_1}^{1-\mu_1} \mathrm{d}\xi_1 \, , \tag{59}$$

replacing,

$$E_4 = \int_{0}^{1} \mathrm{d}\mu_1 \int_{0}^{1-\mu_1} \mathrm{d}z_2 \int_{\mu_1+z_2}^{1} \mathrm{d}s_2 \int_{s_2-\mu_1}^{1-\mu_1} \mathrm{d}\xi_1 \, (...) \, , \tag{60}$$

where the integration in the μ_1, z_2, s_2 coordinates gives the volume of a tetrahedron. Next, performing a cyclic permutation,

$$E_4 = \int_0^1 ds_2 \int_0^{s_2} d\mu_1 \int_0^{s_2-\mu_1} dz_2 \int_{s_2-\mu_1}^{1-\mu_1} d\xi_1 \, (...) \,, \tag{61}$$

and using the fourth Duffy transformation of Table 6 for the E_4 integral, it is

$$E_4 = J_b \int_0^1 d\omega \int_0^1 dx_1 \int_0^1 dx_2 \int_{s_2-\mu_1}^{1-\mu_1} d\xi_1 \, (...) \,. \tag{62}$$

The linear mapping from the interval $s_2 - \mu_1 \leq \xi_1 \leq 1 - \mu_1$ to the $0 \leq \chi_1 \leq 1$ one leads to the dependences expressed by the fourth row of Table 6.

9.5 Integral E_5

Starting from

$$E_5 = \int_{-1}^0 d\mu_1 \int_{-1}^{\mu_1} d\mu_2 \int_{-\mu_2}^1 d\xi_1 \int_{-\mu_2}^{\xi_1} d\xi_2 \, (...) \,, \tag{63}$$

introducing the auxiliary coordinates $z_1 = -\mu_1$ and $z_2 = -\mu_2$,

$$E_5 = \int_0^1 dz_1 \int_{z_1}^1 dz_2 \int_{z_2}^1 d\xi_1 \int_{z_2}^{\xi_1} d\xi_2 \, (...) \,, \tag{64}$$

interchanging the integration order,

$$\int_{z_2}^1 d\xi_1 \int_{z_2}^{\xi_1} d\xi_2 = \int_{z_2}^1 d\xi_2 \int_{\xi_2}^1 d\xi_1 \,, \tag{65}$$

applying the auxiliary coordinate $s_2 = \xi_2$,

$$\int_{z_2}^1 d\xi_2 \int_{\xi_2}^1 d\xi_1 = \int_{z_2}^1 ds_2 \int_{s_2}^1 d\xi_1 \,, \tag{66}$$

and replacing in Eq. (64)

$$E_5 = \int_0^1 dz_1 \int_{z_1}^1 dz_2 \int_{z_2}^1 ds_2 \int_{s_2}^1 d\xi_1 \, (...) \,, \tag{67}$$

where the integration in the z_1, z_2, s_2 coordinates gives the volume of a tetrahedron. By proposing a cyclic permutation,

$$E_5 = \int_0^1 ds_2 \int_{s_2}^1 dz_1 \int_0^{z_1} dz_2 \int_{s_2}^1 d\xi_1 \, (...) \,, \tag{68}$$

and using the fifth Duffy transformation of Table 6 corresponding to the E_5 integral, then

$$E_5 = J_b \int_0^1 d\omega \int_0^1 dx_1 \int_0^1 dx_2 \int_{s_2}^1 d\xi_1 \, (...) \,. \tag{69}$$

Finally, introducing the linear mapping from the interval $s_2 \leq \xi_1 \leq 1$ to the $0 \leq \chi_1 \leq 1$ one, the dependences expressed by the fifth row of Table 6 are obtained.

9.6 Integral E_6

Beginning with

$$E_6 = \int_0^1 d\mu_1 \int_{\mu_1}^1 d\mu_2 \int_{\mu_2-\mu_2}^{1-\mu_1} d\xi_1 \int_0^{\xi_1-\mu_2+\mu_1} d\xi_2 \, (...) \,, \tag{70}$$

interchanging the integration order,

$$\int_{\mu_2-\mu_2}^{1-\mu_1} d\xi_1 \int_0^{\xi_1-\mu_2+\mu_1} d\xi_2 = \int_0^{1-\mu_2} d\xi_2 \int_{\xi_2+\mu_2-\mu_1}^{1-\mu_1} d\xi_1 \,, \tag{71}$$

introducing the auxiliary coordinate $s_2 = \xi_2 + \mu_2$,

$$\int_0^{1-\mu_2} d\xi_2 \int_{\xi_2+\mu_2-\mu_1}^{1-\mu_1} d\xi_1 = \int_{\mu_2}^1 ds_2 \int_{s_2-\mu_1}^{1-\mu_1} d\xi_1 \,, \tag{72}$$

replacing,

$$E_6 = \int_0^1 d\mu_1 \int_{\mu_1}^1 d\mu_2 \int_{\mu_2}^1 ds_2 \int_{s_2-\mu_1}^{1-\mu_1} d\xi_1 \, (...) \,, \tag{73}$$

where the integration in μ_1, μ_2, s_2 coordinates gives the volume of a tetrahedron, then, performing a cyclic permutation,

$$E_6 = \int_0^1 ds_2 \int_{s_2}^1 d\mu_1 \int_0^{s_2} d\mu_2 \int_{s_2-\mu_1}^{1-\mu_1} d\xi_1 \, (...) \,, \tag{74}$$

and using the sixth Duffy transformation of Table 6 corresponding to the E_6 integral, it results

$$E_6 = J_b \int_0^1 d\omega \int_0^1 dx_1 \int_0^1 dx_2 \int_{s_2-\mu_1}^{1-\mu_1} d\xi_1 \, (...) \,. \tag{75}$$

The sixth row of Table 6 is reached by applying the linear mapping from the interval $s_2 - \mu_1 \leq \xi_1 \leq 1 - \mu_1$ to the $0 \leq \chi_1 \leq 1$ one.

REFERENCES

Battaglia L., D'Elía J., Storti M.A., and Nigro N.M. Numerical simulation of transient free surface flows. *ASME-Journal of Applied Mechanics*, 73(6):1017–1025, 2006.

Berry A. A new formulation for the vibrations and sound radiation of fluid-loaded plates with elastic boundary conditions. *J. Acoust. Soc. Am.*, 96(2):889–901, 1994.

Burghignoli P., Pajewski L., Frezza F., and Galli A. Improved quadrature formulas for boundary integral equations with conducting or dielectric edge singularities. *IEEE Trans. on Antennas and Propagation*, 52(2):373–379, 2004.

Dalcín L., Paz R.R., Storti M., and D'Elía J. MPI for Python: Performance Improvements and MPI-2 Extensions. *Journal of Parallel and Distributed Computing*, 68(5):655–662, 2007.

D'Elía J., Nigro N., and Storti M. Numerical simulations of axisymmetric inertial waves in a rotating sphere by finite elements. *International Journal of Computational Fluid Dynamics*, 20(10):673–685, 2006.

D'Elía J., Storti M., and Idelsohn S. A closed form for low order panel methods. *Advances in Engineering Software*, 31(5):335–341, 2000a.

D'Elía J., Storti M., and Idelsohn S. Iterative solution of panel discretizations for potential flows. the modal/multipolar preconditioning. *Int. J. Num. Meth. Fluids*, 32(1):1–27, 2000b.

D'Elía J., Storti M., and Idelsohn S. Applied hydrodynamic wave-resistance computation by Fourier transform. *Ocean Engineering*, 29:261–278, 2002a.

D'Elía J., Storti M., Oñate E., and Idelsohn S. A nonlinear panel method in the time domain for seakeeping flow problems. *Int. J. of Computational Fluid Dynamics*, 16(4):263–275, 2002b.

D'Elía J., Storti M.A., and Idelsohn S.R. A panel-Fourier method for free surface methods. *ASME-Journal of Fluids Engineering*, 122(2):309–317, 2000c.

Duffy M.G. Quadrature over a pyramid or cube of integrands with a singularity at a vertex. *SIAM Journal on Numerical Analysis*, 19(6):1260–1262, 1982.

Eibert T.F. and Hansen V. On the calculation of potential integrals for linear source distributions on triangular domains. *IEEE Trans. on Antennas and Propagation*, 43(12):1499–1502, 1995.

Fachinotti V., Cardona A., D'Elía J., and Paquay S. BEM for the analysis of fluid flow around MEMS. In *Mecánica Computacional, vol. XXIV*, pages 1104–1119. 2007.

Franck G., Nigro N., Storti M., and D'Elía J. Numerical simulation of the Ahmed vehicle model near–wake. *Latin American Applied Research*, 2007. In press.

Garibaldi J., Storti M., Battaglia L., and D'Elía J. Numerical simulations of the flow around a spinning projectil in subsonic regime. *Latin American Applied Research*, 38(3):241–247, 2008.

Hartmann F. *Introduction to Boundary Elements*. Springer-Verlag, 1989.

Kim S. and Karrila S.J. Integral equations of second kind for Stokes flow: direct solutions for physical variables and removal of inherent accuracy limitations. *Chem. Eng. Comm.*, 82:123–161, 1989.

Medina D. and Liggett J. Three-dimensional boundary element computation of potential flow in fractured rock. *Int. J. for Num. Meth. in Eng.*, 26:2319–2330, 1988.

Méndez C., Paquay S., Klapka I., and Raskin J.P. Effect of geometrical nonlinearity on MEMS thermoelastic damping. *Nonlinear Analysis: Real World Applications*, 2008. In press.

Paquay S. *Développement d'une méthodologie de simulation numérique pour les problèmes vibro-acoustiques couplés intérieurs/extérieurs de grandes taille*. Ph.D. thesis, Faculté des Sciences Appliquées, Liège, 2002.

París F. and Cañas J. *Boundary Element Method. Fundamentals and applications*. Oxford Press, 1997.

PETSc-FEM. A general purpose, parallel, multi-physics FEM program, GNU General Public License, http://www.cimec.ceride.gov.ar/petscfem. 2008.

Power H. and Wrobel L. *Boundary Integral Methods in Fluid Mechanics*. Computational Mechanics Publications, Southampton,UK, 1995.

Quarteroni A., Sacco R., and Saleri F. *Numerical Mathematics*. Springer-Verlag, 2000.

Schuhmacher A. *Sound source reconstruction using inverse sound field calculations*. Ph.D. thesis, Department of Acoustic Technology, Technical University of Denamark, 2000.

Sievers D., Eibert T.F., and Hansen V. Correction to "On the calculation of potential integrals for linear source distributions on triangular domains". *IEEE Trans. on Antennas and Propagation*, 53(9):3113–3113, 2005.

Storti M., D'Elía J., and Idelsohn S. Algebraic Discrete Non-Local (DNL) absorbing boundary condition for the ship wave resistance problem. *J. Comp. Physics*, 146(2):570–602, 1998a.

Storti M., D'Elía J., and Idelsohn S. Computing ship wave resistance from wave amplitude with the DNL absorbing boundary condition. *Comm. Numer. Meth. Engng.*, 14:997–1012, 1998b.

Storti M.A. and D'Elía J. Added mass of an oscillating hemisphere at very-low and very-high

frequencies. *ASME, Journal of Fluids Engineering*, 126(6):1048–1053, 2004.

Storti M.A., Nigro N.M., Paz R., and Dalcín L.D. Dynamic boundary conditions in computational fluid dynamics. *Comp. Meth. in Appl. Mech. and Engr.*, 197(13–16):1219–1232, 2008. doi:10.1016/j.cma.2007.10.014. Elsevier, Amsterdam, The Netherlands.

Taylor D.J. Accurate and efficient numerical integration of weakly singulars integrals in Galerkin IFIE solutions. *IEEE Trans. on Antennas and Propagation*, 51(7):1630–1637, 2003a.

Taylor D.J. Errata to "Accurate and efficient numerical integration of weakly singulars integrals in Galerkin IFIE solutions". *IEEE Trans. on Antennas and Propagation*, 51(9):2543–2543, 2003b.

Wang W. and Atalla N. A numerical algorithm for double surface integrals over quadrilaterals with a 1/r singularity. *Communications in Numerical Methods in Engineering*, 13(11):885–890, 1997.

Wang X. *Fast Stokes: A Fast 3-D Fluid Simulation Program for Micro-Electro-Mechanical Systems*. Ph.D. thesis, MIT, 2002.